Physica Scripta

PAPER

High-sensitivity photonic crystal sensor for early detection of atherosclerosis

Farida Kebaili , Abdesselam Hocini and Ahlam Harhouz

Laboratoire d'Analyse des Signaux et Systèmes, Mohamed Boudiaf University of M'sila, Faculty of Technology, Departement of Electronics, 28000 M'slia, Algeria

E-mail: farida.kebaili@univ-msila.dz

RECEIVED
6 March 2025

REVISED
24 April 2025

ACCEPTED FOR PUBLICATION
6 May 2025

PUBLISHED
15 May 2025

Keywords: photonic crystal, biosensor, finite-difference time-domain (FDTD), photonic band gap (PBG)

Abstract

Early detection of atherosclerosis is crucial to preventing its cardiovascular complications. In this study, a 2D-Photonic Crystal (PhC) sensor model was designed and simulated using the RSoft software to optimize diagnostic sensitivity and accuracy. Five configurations of the sensor were explored to evaluate their performance. Structure A emerged as the most efficient, enabling the reliable identification of atherosclerotic plaques (lipidic, fibrous, and calcified) with a high sensitivity of 756.66 nm RIU^{-1}, a quality factor of 1753.4, and a figure of merit of 8.33×10^5 RIU^{-1}. The 2D-PhC structure offers distinct advantages over traditional 1D-PhC sensors, including enhanced light interaction and spectral resolution. Compared to 1D-PhCs, the 2D structure provides improved sensitivity and faster detection, which are crucial for distinguishing healthy tissues from pathological ones. Performance analysis demonstrated that the proposed structure outperforms conventional methods such as Doppler ultrasound and angiography in terms of precision and detection speed. These results demonstrate that optimizing 2D photonic crystal microcavities, supported by advanced simulations with RSoft, significantly enhances the detection of cardiovascular diseases. This sensor could be integrated into non-invasive diagnostic devices, contributing to the advancement of current medical technologies.

1. Introduction

Atherosclerosis is a complex and potentially life-threatening cardiovascular disease characterized by the progressive accumulation of plaques in arterial walls [1]. These plaques, composed of lipids, inflammatory cells, and fibrotic tissue, contribute to the narrowing and stiffening of blood vessels, significantly increasing the risk of myocardial infarction, stroke, and other cardiovascular complications [2]. Despite advances in treatment and management, cardiovascular diseases remain a leading cause of mortality worldwide, underscoring the need for effective prevention, early detection, and intervention strategies [3].

The pathological progression of atherosclerosis begins with endothelial dysfunction and lipid accumulation, which trigger inflammatory responses and tissue remodeling [4]. Over time, these processes lead to the formation of distinct types of plaques, including lipid-rich [5], fibrous, and calcified lesions, each associated with different stages of the disease. Early detection of these plaques is critical, as it enables timely interventions to slow disease progression, reduce complications, and improve patient outcomes [6]. However, conventional diagnostic methods, such as angiography and ultrasonography, face limitations in sensitivity, specificity, and accessibility, highlighting the demand for innovative diagnostic technologies [7].

The field of optics and photonics has witnessed significant advancements in the development of various optical devices that have transformed diagnostic practices. For instance, optical demultiplexers [8], interferometers [9], optical couplers [10], sensors [11], and even logic gates [12] are increasingly being employed across various fields, ranging from telecommunications to medical diagnostics. Photonic crystal (PC) sensors, in particular, have garnered attention for their exceptional sensitivity and ability to detect minute changes in the optical properties of biological samples [13]. These sensors are engineered using periodic dielectric structures

that create photonic band gaps [14], allowing them to manipulate light in ways that surpass conventional optical systems [15]. The high sensitivity of photonic crystal sensors to refractive index variations makes them ideal for identifying changes in arterial tissue composition associated with atherosclerotic plaque formation [16].

Recent studies have also explored one-dimensional (1D) and two-dimensional (2D) photonic crystals for sensing applications. For example, 1D photonic crystals have been used to enhance sensitivity in various biosensing applications [17]. Two-dimensional photonic crystals, on the other hand, offer superior control over light propagation and are increasingly being employed to improve detection capabilities in medical diagnostics [18]. These structures, by providing stronger confinement of light, show a marked advantage over traditional sensor designs, particularly in terms of enhanced sensitivity and resolution [19].

This study explores the design and simulation of a high-sensitivity photonic crystal sensor for the early detection of atherosclerosis. By leveraging the unique optical properties of photonic crystals, this sensor can analyze refractive index variations in arterial tissues, distinguishing between healthy arterial walls and different types of plaques—lipid-rich, fibrous, and calcified. The refractive indices, which range from 1.38 to 1.65 depending on the tissue composition, serve as key optical markers for identifying the type and stage of atherosclerotic lesions [1].

Through simulation using RSOFT software, this research validates the potential of photonic crystal sensors as a cutting-edge tool for early and non-invasive detection of atherosclerosis. Our photonic crystal-based microcavity sensor offers several key advantages over traditional methods. It achieves a sensitivity of 756.66 nm RIU^{-1}, which is significantly higher than conventional optical sensors used in medical imaging, where sensitivity typically ranges from 1–100 nm RIU^{-1}. Unlike Doppler ultrasound and angiography [20], which detect blood flow variations and vascular structures but are not directly sensitive to subtle refractive index variations in tissues, our sensor provides direct refractive index detection. Additionally, it can accurately differentiate atherosclerotic plaques—lipid-rich, fibrous, and calcified—based on refractive index variations with high spectral resolution. In contrast, Doppler ultrasound relies on indirect blood flow measurements [21], which can be affected by motion artifacts, while angiography requires the injection of contrast agents and exposes patients to X-ray radiation, our approach offers a non-invasive detection method with fine spectral resolution [22]. Our simulations indicate that the sensor's response time could be on the order of milliseconds, making it significantly faster than angiography, which involves preparation, injection, and image analysis. Furthermore, in terms of cost, an integrated optical sensor in a compact device could provide a more affordable alternative to large medical equipment that requires highly trained personnel and hospital infrastructure [23].

2. Structure design and analysis method

2.1. Photonic band diagram

Numerical techniques were employed to design and simulate the proposed optical sensor [24]. The plane wave expansion (PWE) method was selected to determine the photonic band gap (PBG) of the initial photonic crystal (PC) structure [25], owing to its ability to accurately calculate PBGs. Additionally, the finite-difference time-domain (FDTD) method was utilized to analyze and validate the simulated structure [26].

In this study, the Plane Wave Expansion (PWE) method was used to calculate the photonic band gap (PBG) with its accuracy depending on the number of plane waves considered—higher numbers yielding more precise results [27]. The hexagonal lattice structure described (20×15 holes with a lattice constant of 0.54 μm) suggests that a sufficiently large basis set was employed to capture the periodicity. In photonic crystal simulations, it is common practice to use 16–32 plane waves per lattice vector for basic structures. In our work, this parameter was optimized based on RSoft's software defaults, which set it to 16 plane waves per lattice vector for basic structures.

We employed the Finite-Difference Time-Domain (FDTD) method using RSoft FullWAVE to validate the sensor design, optimizing the setup for accuracy and computational efficiency [28]. Perfectly Matched Layers (PMLs) were likely used to absorb outgoing waves and minimize reflections, as is standard in PhC simulations [29], and the transmission spectra in figure 3 suggest minimal spurious reflections, indicating effective PML implementation. Periodic boundary conditions might have been applied in the transverse directions (parallel to the PhC lattice) to model infinite periodicity, though this is not explicitly stated. The mesh resolution is critical for resolving subwavelength features such as air holes with a radius of $r = 240$ nm, and a typical rule of thumb for mesh size is $\Delta x = \lambda min/(10\ n)$, where n is the refractive index. For the TM-mode wavelength range (1.1225–1.8711 μm) and a silicon background ($n = 3.45$), this suggests a mesh size of approximately 20–30 nm. The Courant-Friedrichs-Lewy (CFL) condition dictates the time step as [30]:

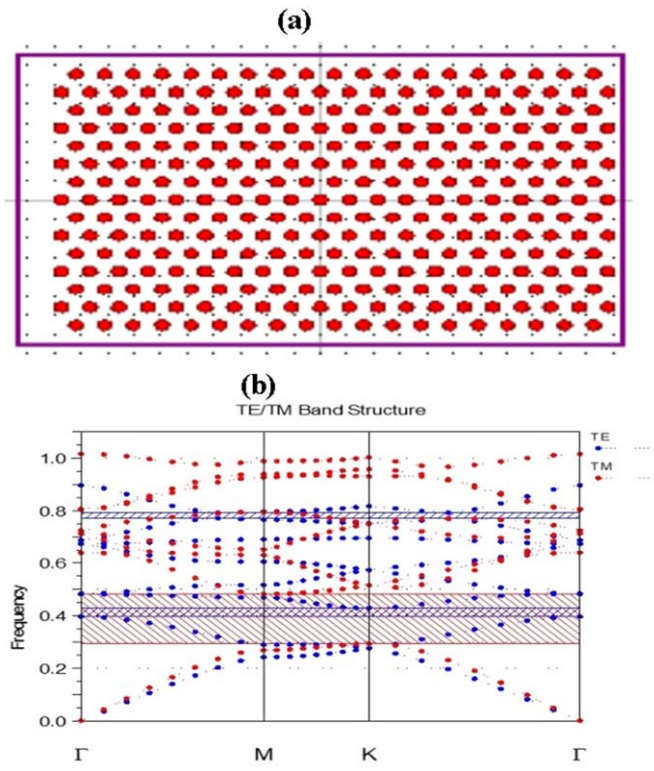

Figure 1. (a) Schematic of the proposed 2D-PhC structure, (b) Band diagram of the proposed 2D-PhC structure.

$$\Delta t \leqslant c \Big/ \sqrt{\left(\frac{1}{\Delta x^2}\right) + \left(\frac{1}{\Delta y^2}\right)} \tag{1}$$

Where c is the speed of light. To maintain numerical stability and ensure convergence, we set $\Delta t = 0.99 \times (\Delta x/c)$, providing an optimal balance between accuracy and simulation speed. Optimizations included mesh refinement (resonance shift $<0.1\%$), convergence testing, and PML efficiency validation, enabling high accuracy with controlled computational costs.

The initial sensor design consists of a hexagonal lattice of 20 rows and 15 columns of air holes in a silicon slab, with a lattice constant of 0.54 μm and a hole radius of 0.24 μm. This structure exhibits two photonic band gaps (PBGs) in the TE mode and one in the TM mode, with the TM mode covering a wavelength range from 1.1225 to 1.8711 μm, making it particularly suitable for electronic and telecommunication applications.

The band structure for the guided mode is depicted in figure 1. The wavelength range for the TM mode was calculated using the formula:

$$\lambda = \frac{a}{v} = \frac{0.54}{0.2886} = 1.8711\ \mu m \tag{2}$$

$$\lambda = \frac{a}{v} = \frac{0.42}{0.48105} = 1.1225\ \mu m \tag{3}$$

where a represents the lattice period of the photonic crystal (PhC), defining the periodicity of the structure, and v is the reduced frequency, which is a dimensionless parameter used for normalization. This formulation allows for a more general analysis independent of the absolute scale of the structure.

2.2. Different sensor design

The sensor structure, at the nanoscale, consists of 20 × 15 holes in the X-Z plane, formed by circular air holes in a silicon background with a hexagonal lattice arrangement, as illustrated in figure 1(a). The air holes have a refractive index (RI) of 1, while the background has an RI of 3.45. As the light signal enters through the input port and traverses the resonator, the waveguides direct the holes carrying the optical signal to the output port. features a hexagonal cavity between two waveguides. These waveguides are created by removing two rows of 3 air holes on left side and 4 air holes on right, each characterized by a radius r = 240 nm, along the ΓK direction on either side of the central cavity. They facilitate the coupling of light both inside and outside the photonic crystal cavity (CPh). The central cavity is composed of 2 Vertical micro cavities. For a detailed view of the sensor's cross-sectional representation, please refer to figure 2(A). The structure is designed with four different hole radius,

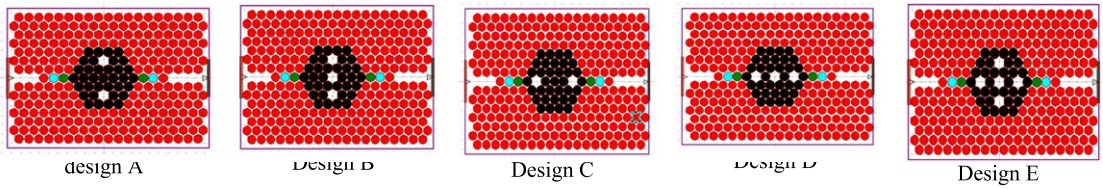

Figure 2. The different physical structure of the proposed biosensor designs.

distinguished by their colors: black ,green, red, and blue cyan , with respective values of 270 nm, 260 nm, 250 nm and 240 nm, selected after optimization of the structural parameters. From this initial structure, we developed other designs by modifying the number and position of the micro cavities as shown in figures 2(B)–(D). Some modifications involve placing the micro cavities vertically or horizontally, while the final design is a combination of both configurations see figure 2(E).

During the simulation, a Gaussian light source with a central frequency and width matching the photonic band gap was placed on the left side of the sensor system and allowed to propagate over multiple periods. The transmission spectrum was monitored by observing the output pulse on the opposite side of the sensor. The excitation light travels from the first waveguide to the second through the cavity and is then detected at the output. This type of coupling allows the extraction of one or several frequencies from the input guide, which can then be redirected towards the second guide.

3. Device operation and results

Several numerical and measurable properties characterize the quality of a refractive index sensor. In this review, we'll examine some of these key properties [31].

3.1. Sensitivity

The term 'sensitivity' is employed to describe sensors that exhibit a shift in resonance wavelength when subjected to varying refractive indexes. If we consider that the interaction between the analyte and bio-receptor leads to a change in refractive index represented by Δn, sensitivity can be defined as shown in equation (4).

$$S = \frac{\Delta\lambda}{\Delta n} \tag{4}$$

3.2. Quality factor

The quality factor, denoted as Q, represents the ratio of the resonance wavelength to the bandwidth measured at full width half maximum (FWHM). It serves as a parameter to characterize the field confinement within a cavity. Achieving a higher sensitivity requires maximizing the quality factor. Equation (5) provides the definition of the quality factor.

$$Q = \frac{\lambda(\text{resonance})}{\Delta\lambda(\text{FWHM})} \tag{5}$$

3.3. Minimum detection limit

The detection limit (DL) is defined based on product of quality factor and sensitivity:

$$DL = \frac{K\omega_0}{Q * S} \tag{6}$$

where, K is the proportionality constant. It is based on the spectral line shape and signal-to-noise ratio (SNR) of the measurement system. Consequently, to have a good biosensor a small DL is required.

3.4. Figure of merite

When assessing the performance of biosensors, a crucial parameter is the figure of merit (FOM). This metric is typically determined by dividing the sensitivity of the biosensor by its FWHM bandwidth. Equation (7) provides the formal definition of the figure of merit.

Table 1. Resonant wavelength and sensitivity for different refractive index values (1.00 to 1.03, step of 0.01) across five design configurations.

Design	Resonant wavelength/sensitivity		
	n	λ[nm]	S[nm/RIU]
Design A	1	1732.4/1782.8	Ref
	1.01	1740.3/1788.2	784/542
	1.02	1747.9/1794.0	772.25/559.75
	1.03	1755.9/1798.9	780.83/536.9
Design B	1	1725.7/1753.1	Ref
	1.01	1732.2/1760.6	650/750
	1.02	1738.6/1768.1	645/750
	1.03	1745.1/1775.4	646.66/743
Design C	1	1254.9	Ref
	1.01	1256.7	180
	1.02	1258.4	175
	1.03	1260.3	182.66
Design D	1	1254.7	Ref
	1.01	1256.2	150
	1.02	1258.6	145
	1.03	1259.0	143.33
Design E	1	1839.5	Ref
	1.01	1845.9	640
	1.02	1852.2	635
	1.03	1858.6	636.66

$$\mathrm{FOM} = \frac{\mathrm{S}}{\mathrm{FWHM}} \tag{7}$$

The transmission in a photonic crystal sensor can be described by the following formula, which expresses the transmission coefficient T as the ratio of the transmitted light intensity ItransmittedItransmitted to the incident light intensity IincidentIincident:

$$\mathrm{T} = \frac{\mathrm{I}_{\mathrm{transmitted}}}{\mathrm{I}_{\mathrm{incident}}} \tag{8}$$

Where:

$\mathrm{I}_{\mathrm{transmitted}}$ is the intensity of the transmitted light,

$\mathrm{I}_{\mathrm{incident}}$ is the intensity of the incident light,

T is the transmission coefficient.

In table 1, we show the performance parameters for the five-sensor design, such as the resonance wavelength and sensitivity.

From the results reported in the table 1, it can be seen that designs using vertical micro cavities tend to offer better sensitivity thanks to the increased depth of resonant modes, which promotes closer interaction between light and the sensing medium and improves the ability to detect small variations. Design B, while having a wide range of resonant wavelengths, has a rather modest sensitivity (645 to 750 nm), which may limit its ability to detect fine variations in the medium. In comparison, Design A stands out for its greater sensitivity and a wavelength range better suited to accurate detection. Designs C, D and E, with their limited or unspecified sensitivity, are also less suitable. Thus, Design A is the recommended choice for atherosclerosis detection, due to its superior sensitivity and performance tailored to precise detection needs.

Figure 3 illustrates the out put spectrum of aproposed sensor under varying configurations using vertical and horizontal micro cavities . Design A stands out from the other configurations due to the presence of two well-defined resonant modes, characterized by narrow peaks and higher amplitude in the transmission spectrum. These features reflect better peak sharpness, achieved through effective optical confinement in the vertical microcavities and strong interaction between light and the sensing medium.

The full width at half maximum (FWHM) of the peaks is significantly reduced in Design A compared to the other designs, enhancing the sensor's spectral resolution and sensitivity. This narrowness allows for the precise detection of minute variations in the refractive index, a critical criterion for distinguishing healthy tissues from atherosclerotic plaques. Furthermore, the dual resonance of Design A broadens its functional range, increasing its versatility in detecting changes across various environments. In comparison, the alternative designs exhibit broader or less pronounced peaks, indicating lower sensitivity and detection efficiency.

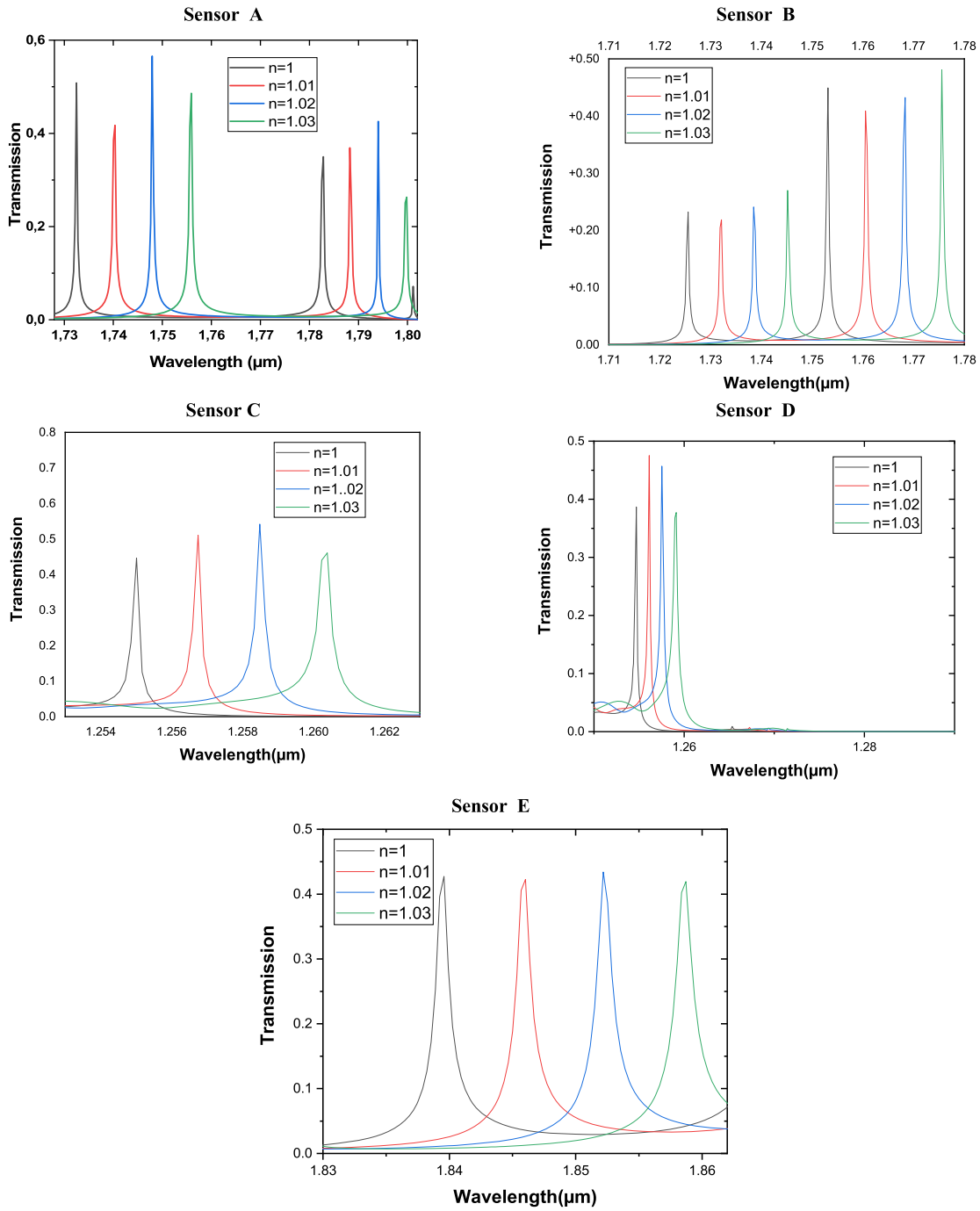

Figure 3. The transmission spectrum of the five proposed sensor A, B, C, D, E respectively.

These observations confirm the superiority of Design A for biomedical applications requiring fast and accurate detection.

Table 2, illustrates the response of the proposed sensor (design A) to both healthy and atherosclerotic tissues. As observed, the sensor exhibits significant wavelength shifts for various types of atherosclerotic tissues. The results indicate that the sensitivity is approximately 756.66 nm RIU^{-1}.

Additionally, the biosensor demonstrates a Q-factor exceeding 1753.4 and a FOM above $8.33^{*}10^{5}$ RIU^{-1}, which are highly promising for atherosclerosis detection when compared to other studies in the field.

The variation in transmission with wavelength for different refractive index values is presented in figure 4. The transmission of light through atherosclerotic tissues depends on their refractive index, which can vary according to the tissue composition. When this index changes, the wavelength at which light is best transmitted shifts. This shift indicates that the optical properties of the tissues influence how light propagates through them. This relationship between the refractive index and transmission is essential for imaging and diagnostic techniques, as it helps to better understand the internal structure of the tissues.

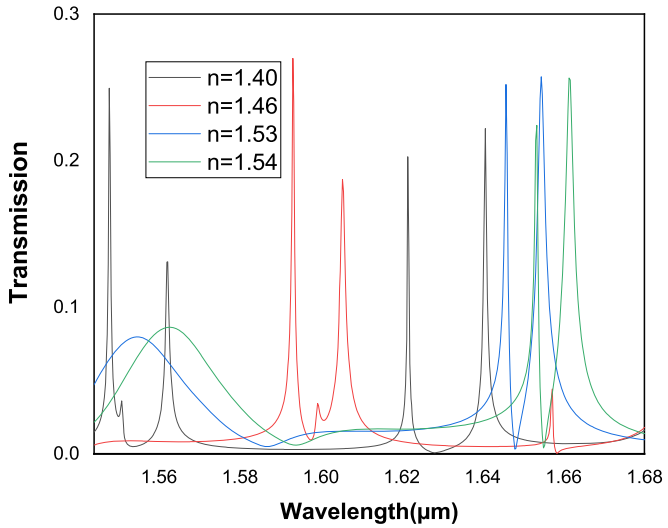

Figure 4. The sensor's transmission spectra in the presence of various types of atherosclerotic tissues.

Table 2. The value of resonant wavelength, Q-factor, sensitivity, DL and FOM of the normal tissues and atherosclerotic plaques.

	Characteristic parameters					
Plaque type	n	λ[nm]	S[nm/RIU]	Q	FOM[RIU^{-1}]*10^5	FWHM[nm]
Healthy arterial tissue	1.40	1547.7/1562.0	/			
Lipid plaque	1.46	1593.1/1605.3	756.66/721.66	1753.4/1753.4	8.33/7.88	0.908577/0.915535
Fibrous tissue	1.53	1645.8/1654.5	754.62/711.54	1032/1031.8	4.73/4.44	1.59476/1.60350
Calcified plaque	1.54	1653.4/1661.6	755/711.43	953.90/954.42	4.36/4.09	1.73330/1.74095

Table 3. Comparison of the proposed biosensor with various similar PhC designs.

References	S[nm/RIU]	Year of publication
[14]	303.65	2020
[16]	702.35	2024
[21]	739	2019
[24]	718.6	2022
[25]	32	2024
[26]	455.33	2023
[29]	688.16	2023
Our work	756	/

In contrast to previous work cited in the literature, our biosensor stands out with significantly higher sensitivity, as shown in the comparative table 3. This improvement represents a major advancement, making our design more precise and reliable for real-time detection, particularly in point-of-care applications.

4. Conclusions

In this study, a 2D photonic crystal-based biosensor is developed and simulated for detecting atherosclerosis. The biosensor's design and performance are analyzed using the Plane Wave Expansion (PWE) method and the Finite-Difference Time-Domain (FDTD) tool within the RSoft Photonic Suite CAD. Detection is based on observing shifts in the transmission spectrum corresponding to various refractive index (RI) changes, which signal the presence of atherosclerotic plaques. By measuring the wavelength shift in response to RI variations, different plaque types can be identified. The design's simplicity allows for easy integration into biochips for medical applications. The findings show that analyzing the transmission spectrum enables straightforward detection of plaques, with the biosensor achieving a sensitivity of 756.66 nm RIU^{-1}, a Q-factor 1753.4 and a

FOM 8.33*10^5 RIU^{-1}. This research explores the design of five distinct biosensors, differing in the placement of microcavities, to evaluate their impact on sensitivity. Simulations demonstrate that the vertical placement of microcavities significantly affects sensitivity. The proposed biosensor offers enhanced accuracy and precision in distinguishing malignant from healthy tissues, making it ideal for real-time point-of-care applications.

Data availability statement

All data that support the findings of this study are included within the article (and any supplementary files).

ORCID iDs

Farida Kebaili https://orcid.org/0000-0003-2923-0291
Abdesselam Hocini https://orcid.org/0000-0002-7602-6210
Ahlam Harhouz https://orcid.org/0000-0003-1677-0950

References

[1] Dirckx J J J, Kuypers L C and Decraemer W F 2005 Refractive index of tissue measured with confocal microscopy *J. Biomed. Opt.* **10** 044014
[2] Schmitt C X J M, Carlier S G and Virmani R 2008 Characterization of atherosclerosis plaques by measuring both backscattering and attenuation coefficients in optical coherence tomography *J. Biomed. Opt.* **13** 034003
[3] Choi S S S, Lashkari B, Mandelis A, Weyers J J, Boyes A, foster S F and Courtney N A K B 2019 Interference-free detection of lipid-laden atherosclerotic plaques by 3D Co-registration of frequency domain differential photoacoustic and ultrasound radar imaging *Sci. Rep.* **9** 12400
[4] Qureshia A, Gurbuzb Y and Niazia J H 2012 Biosensors for cardiac biomarkers detection. *A review Sensors Actuators B* **171–172** 62–76
[5] Shi C, Xie H, Ma Y, Yang Z and Zhang J 2020 Nanoscale technologies in highly sensitive diagnosis of cardiovascular diseases *Front. Bioeng. Biotechnol.* **8** 531
[6] Sandeman R C L, Nankivell V, Tan J T M, Rashidi M, Psaltis P J, Zheng G, Bursill C, McLaughlin R A and Li J 2024 Detection of atherosclerotic plaques with HDL like porphyrin nanoparticles using an intravascular dual modality optical coherence tomography and fluorescence system *Sci. Rep.* **14** 12359
[7] Xue J *et al* 2023 Ultra-high sensitivity terahertz microstructured fiber biosensor for diabetes mellitus and coronary heart disease marker detection *Sensors* **23** 2020
[8] Shiva K, Ali F and Ali M 2021 Reconfigurable and scalable 2,4-and 6-channel plasmonics demultiplexer utilizing symmetrical rectangular resonators containing silver nano-rod defects with FDTD method *Sci. Rep.* **11** 13628
[9] Muhammad A B, Muhammad S and Ryszard P 2023 Racetrack ring resonator integrated with multimode interferometer structure based on low-cost silica-titania platform for refractive index sensing *Photonics* **10** 978
[10] Jie, T, Shuqing Y, Wei Y and Min Q 2009 Broadband high-efficiency surface-plasmon-polariton coupler with silicon-metal interface *Appl. Phys. Lett.* **95** 013504
[11] Rizwanur R, Md Alam H and Nazmul H 2024 Numerical investigation of a highly sensitive plasmonic refractive index sensor for the detection of breast and cervical cancer biomarkers *Plasmonics* (https://doi.org/10.1007/s11468-024-02565-1)
[12] Mohammed J A, Mithaq N R and Ali A A 2023 Nanoscale plasmonic logic gates design by using an elliptical resonator *Appl. Opt.* **62** 4080–9
[13] Kebaili F, Harhouz A and Hocini A 2024 Modeling and simulation of photonic crystal sensor for drinking water quality monitoring *Progress In Electromagnetics Research C* **40** 85–91
[14] Qi C, Shutao W, Jiangtao L, Na L and Bo P 2020 Refractive index sensor based on photonic crystal nanocavity *Opt. Commun.* 1–9
[15] Defvi E F and Rahmasari L 2023 Photonic crystals based biosensors in various biomolecules applications *Review, Physics Communication* **7** 80–90
[16] Harhouz A, Tayoub H and Hocini A 2024 Multiple fano resonator based on photonic crystal waveguide coupled with two micro-cavities for biomedical sensing application *Phys. Scr.* **99** 055545
[17] Kamenev A O, Vanyushkin N A, Efimov I M and Gevorgyan A H 2025 One-dimensional photonic crystals with two defects: An analytical approach *Optik* 172231
[18] Sharma P and Medhekar S 2024 Fluid nonlinear coefficient sensor designed on 2D photonic crystal *J. Opt.* 4616–22
[19] Mahmoodi Y and Fathi D 2021 High-performance refractive index sensor for oil derivatives based on MWCNT photonic crystal microcavity *Opt. Laser Technol.* **138** 106865
[20] Yang Y, Xiang Y and Qi X 2023 Design of photonic crystal biosensors for cancer cell detection *Micromachines* **14** 1478
[21] Rahman-Zadeha F, Danaieb M and Kaatuziana H 2019 Design of a highly sensitive photonic crystal refractive index sensor incorporating ring-shaped GaAs cavity *Opto-Electron. Rev.* **27** 369–77
[22] Zhang A, Yang X and Wang J 2024 Design of channel drop filters based on photonic crystal with a dielectric column with large radius inside ring resonator *Photonics* **11** 554
[23] Muhammad S, Chen D, Xian C, Zhou J, Lei Z, Kuang P, Li Z, Wen G and Huang Y 2024 Design and fabrication of high-quality two-dimensional silicon-based photonic crystal optical cavity with integrated waveguides *Photonics* **11** 753
[24] Khani S and Hayati M 2022 Optical biosensors using plasmonic and photonic crystal band gap structures for the detection of basal cell cancer *Sci. Rep.* **12** 5246
[25] Heidari F, Parandin F, Boochani A, Rahimi Z and Parandin M M 2024 Design of a two dimensional photonic crystal biosensor to identify blood cholesterol in humans *Discover Electronics* **1** 14
[26] Badawi K A, Hamed M M and Mohammed N A 2023 An innovative biosensor harnessing the potential of photonic crystal technology to identify a multitude of cancer cells, distinguished by heightened quality factor and sensitivity *J. Opt.* (https://doi.org/10.1007/s12596-023-01524-z)

[27] Britto E C, Krishnamoorthi B, Rajasekar R and Mohamed Nizar S 2024 Photonic crystal–based nanoscale multipurpose biosensor for detection of brain tumours, hiv, and anaemia with high sensitivity *Plasmonics* (https://doi.org/10.1007/s11468-024-02199-3)
[28] Harshitha V S and Rohan R 2024 Design and analysis of optically sensitive biosensor using two dimensional photonic crystal for oral cancerous cell detection *J. Opt.* (https://doi.org/10.1007/s12596-023-01619-7)
[29] Tayoub H, Harhouz A and Hocini A 2023 2D photonic crystal biosensing platform based on coupled defective ring-shaped microcavity-two waveguides for diabetes detection using human tears *Phys. Scr.* **98** 115510
[30] Kumar B M H, Vaibhav A M and Srikanth P C 2022 Si/SiO_2 Based nano-cavity biosensor for detection of anemia, hiv and cholesterol using refractive index of blood sample *Indian Journal of Science and Technology* **15** 899–907
[31] Fallahi V, Kordrostami Z and Hosseini M 2024 Cancer detection by photonic crystal optical biosensors: effect of hexagonal micro ring resonator design *Mater. Sci. Semicond. Process.* **174** 108188